J. Vis. Commun. Image R. 46 (2017) 23–32

Contents lists available at ScienceDirect

J. Vis. Commun. Image R.

journal homepage: www.elsevier.com/locate/jvci

Perceptually lossless coder for volumetric medical image data ☆

B.K. Chandrika [a,*], P. Aparna [b], David S. Sumam [b]

[a] Manipal University, Manipal Institute of Technology, Department of Electrical and Electronics Engineering, 576104, India
[b] National Institute of Technology Karnataka, Department of Electronics and Communication Engineering, Surathkal 575025, India

ARTICLE INFO

Article history:
Received 1 September 2016
Revised 2 January 2017
Accepted 3 March 2017
Available online 6 March 2017

Keywords:
Image compression
Visual perception
Human visual system
Bilateral symmetry
MRI and CT images

ABSTRACT

With the development of modern imaging techniques, every medical examination would result in a huge volume of image data. Analysis, storage and/or transmission of these data demands high compression without any loss of diagnostically significant data. Although, various 3-D compression techniques have been proposed, they have not been able to meet the current requirements. This paper proposes a novel method to compress 3-D medical images based on human vision model to remove visually insignificant information. The block matching algorithm applied to exploit the anatomical symmetry remove the spatial redundancies. The results obtained are compared with those of lossless compression techniques. The results show better compression without any degradation in visual quality. The rate-distortion performance of the proposed coders is compared with that of the state-of-the-art lossy coders. The subjective evaluation performed by the medical experts confirms that the visual quality of the reconstructed image is excellent.

1. Introduction

In recent years, advancement in imaging modalities like MRI, CT, and Positron Emission Tomography (PET) has greatly influenced the diagnosis and treatment of diseases. Early detection and accurate diagnosis of a medical condition calls for improved quality and quantity of medical data. Thus, increase in image resolution, data volume and improved inter-slice distance results in an enormous volume of image data. Analysis and diagnosis require storage of data. For applications such as tele-medicine and teleradiology, it is often required to transmit the data over long distance communication channel in shortest possible time. Thus, it is very crucial to compress these huge volume of medical image data for storage and/or transmission. On the other hand, these medical data cannot afford to lose any visually significant information which otherwise would lead to wrong diagnosis of any critical pathological condition. Hence, it is important to maintain a balance between compression efficiency and the quality of the reconstructed image data.

A number of 2-D medical image compression algorithms have been reported in literature that treat each slice independently and compress the image one by one. The inter-slice distance would typically vary from 5 mm to 0.5 mm in current technologies required to exploit the inter-slice redundancy. To cope with the compression requirements, it is very important to extend the compression technique to volumetric MRI data, thus addressing the inter-slice correlation. A number of 3-D lossless compression involving prediction techniques and 3-D transformations are available in the literature to eliminate slice correlation for volumetric medical image data. Taquet [1] used Part-2 of Joint Photographic Experts Group (JPEG) 2000 to compress medical image by exploiting the correlation among adjacent images. In this, 1-D reversible 5/3 wavelet transform is applied across image slices for the entire volume followed by JPEG 2000 on the resulting transformed slices. In [2], all MRI slices are de-correlated using lossless Karhunen Loeve Transform (KLT) to exploit inter-slice redundancy. Later, spatial redundancy of each KLT slice is eliminated by applying JPEG-LS image coder. Menegaz and Thiran [3] also focused on the development of a fully 3-D wavelet based coding system featuring 3-D encoding/2-D decoding functionality.

Since most of the medical image slices are relatively symmetrical, Sanchez et al. [4] implemented a compression algorithm which exploits the anatomical symmetries present in the structural medical images. They used 2-D Integer Wavelet Transform (IWT) to de-correlate the data, an intraband prediction method to reduce the energy of the sub-bands exploiting the inherent symmetry present in the medical image and an embedded block coder to achieve high lossless compression gain. This algorithm was modified by adding an inter-slice differential pulse-code modulation prediction method to exploit the correlation between slices [5]. Amraee et al.

☆ This paper has been recommended for acceptance by Zicheng Liu.

* Corresponding author.
E-mail address: chandrika.bk@manipal.edu (B.K. Chandrika).

http://dx.doi.org/10.1016/j.jvcir.2017.03.006
1047-3203/

[6] eliminates both intra-slice and inter-slice correlations with block matching routines considering symmetrical characteristics of these images. To eliminate inter-slice correlation, authors have first predicted the pixels of one half of the image, using the corresponding pixels in the other half based on symmetric nature of medical image. To exploit inter-slice correlations, successive slices are paired and the same method is applied. Pizzolante et al. [7] have suggested a low complexity, reversible 3-D compression algorithm for CT and MRI slices that exploits spatial and slice redundancy using 3-D linear prediction.

Lossless or reversible compression techniques are more preferred by medical professionals as every detail that can be perceived by a medical expert is very significant in the diagnosis of any pathological condition. However, lossless methods for compression of medical images reported in literature including JPEG-Lossless (JPEG-LS) [8,9] don't promise good compression efficiency. On the other hand, a number of lossy methods have been proposed that provide high compression but at the cost of quality degradation which is unacceptable by the medical experts. High Efficiency Video Coding (HEVC) is a new standard for video compression. Performance of this video coding is superior to other video coding standards [10,11]. Hence, this technique is also applied to medical images in picture archiving and communications systems (PACS) [12,13]. However many times HEVC is required to operate at higher bitrates to meet the quality constraint.

So majority of the lossless or lossy compression algorithms available for medical image data do not completely fulfill the quality-compression requirement. Hence, there is a need to have an intermediate system with compression efficiency close to that of lossy and quality close to that of lossless compression system. This can be achieved easily by exploiting HVS characteristics to remove visually insignificant data without losing any diagnostically significant data. But vision based compression of medical images, is still a major challenge. The paper by Wu et al. [14] used this approach to compress MRI, CT and computed radiography medical images by embedding visual pruning function into JPEG 2000 coding framework. However this coding technique is developed for 2-D medical images.

From the above study, it has been observed that there is a need to propose a novel method that would combine removal of symmetrical redundancies, removal of inter-slice redundancies, and at the same time removal of visually/diagnostically insignificant data based on HVS. With this in mind, we have proposed a novel technique based on human perception that guarantees a quality very much close to that of lossless methods and at the same time low bitrates close to that of lossy methods. The proposed perceptually lossless image coding (PLIC) provides greater compression gain than lossless coding schemes while producing images without any visible loss. The proposed perceptually lossless compression method for 3-D MRI and CT image data embeds Just Noticeable Distortion (JND) profile with symmetry based lossless image compression technique different from [14] to remove visually redundant information. In the proposed method, two types of JND models are combined with block matching algorithm and their performances are compared. Along with this, we also compare the results with lossless compression techniques. Rest of the paper is structured as follows. Symmetry based perceptually lossless image coder (PLIC) is discussed in Section 2, in which background luminance and texture based JND models are used to eliminate perceptual redundant information. Simulation results are given in Section 3.

2. Proposed method

Block diagram of the proposed method consisting of Quantizer, Symmetry detector, JND profile estimator, Inter-slice block matching, Intra-slice block matching and Arithmetic coding is shown in Fig. 1. Detailed explanation of each of these blocks is presented in the following subsections.

Proposed JND profile estimator calculates the visibility threshold value for all the image slices in spatial domain. This quantizer removes the visually redundant data. A block matching unit following this removes the inter-slice redundancy. Symmetry detector block checks the presence of symmetry in each slice and if present would feed it to the intra-slice block matching unit. Intra-slice block match routine is applied on residual data of each slice to improve bit rate if symmetry is present in the image plane. Finally, the image residue and the displacement vectors generated by block matching are compressed using arithmetic coding. A feedback from the reconstructed image is used for computing the Visual Information Fidelity (VIF) which is used to fix the quantization weighting factor q_0 as explained in Section 2.2. This algorithm is simulated with two types of JND estimators as explained below.

2.1. JND profile estimator

Medical image compression demands for high visual quality close to that of lossless methods for medical examination. At the same time, good compression efficiency like lossy methods are also desirable. To achieve high visual quality with good compression performance, it is very important to utilize the HVS characteristics. Exploiting HVS characteristic guarantees removal of visually insignificant data without altering any diagnostically significant data. JND profile is employed to exploit these perceptual/visual redundancies which provides a visibility threshold of distortion for each pixel. Reconstruction errors in the images are unnoticeable below this threshold. Among the available spatial domain and transform domain JND models in the literature [15], two spatial domain JND models are used in this work.Visibility threshold in first model (JND model-1) is dependent on average background luminance around the pixel and spatial gradient in the background luminance. Visibility threshold in second model (JND model-2) is

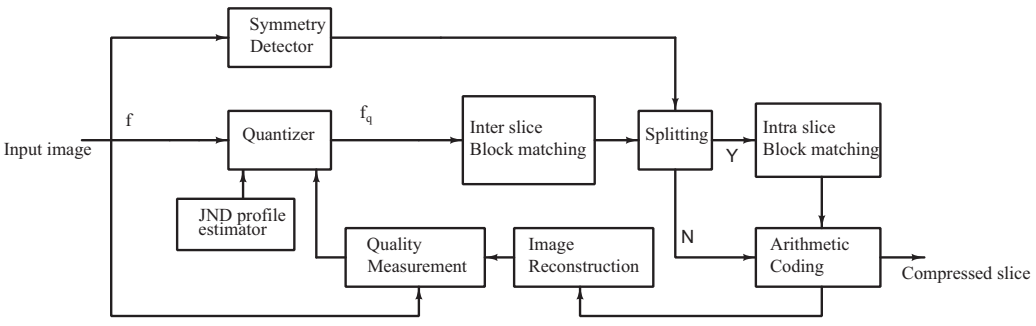

Fig. 1. Block diagram of the proposed method.

dependent on average background luminance, spatial luminance gradient and texture masking.

2.1.1. JND Model-1

Perceptual redundancies present in images are primarily due to the disparity in sensitivity of HVS to the differing levels of contrast and luminance variation in the spatial domain. While applying the feature of HVS to the image, the visibility threshold is the most important measure for expressing perceptual redundancy. Visibility threshold of coding deformity is the magnitude of the stimulus at which degradation becomes just visible or just unnoticeable. The visibility threshold for gray scale images depend on many factors.

Among them, two factors namely *Average Background Luminance around the pixel to be considered* and *Spatial Variation in the background luminance* basically affect the images in the spatial domain. Regarding the first factor, it has been proved that human visual perception is sensitive to luminance contrast rather than the absolute luminance value [16]. Due to the presence of ambient illumination surrounding the display, the distortion in very dark regions tend to be less seen than that is present in regions of better luminance. According to Weber's law, with lower background luminance, the Weber fraction (the ratio of just noticeable luminance difference to stimulus luminance) increases as the background luminance decreases. In the case where the background luminance is high, the Weber fraction remains constant with the increasing background luminance. So high perceptibility threshold is assigned to either very bright or dark areas and low values in regions of medium gray values [17]. The second factor indicates that the increase in the spatial heterogeneity in the background luminance reduces the visibility of stimuli which is referred as spatial masking.

In our work, the pixel based perceptual model [18] has been selected to measure the perceptual redundancy that depend on the above discussed factors which are computed for every pixel. Average background luminance $bl(x,y)$ and maximum weighted gradient of average background luminance $wg(x,y)$ surrounding the pixel $p(x,y)$ are defined as follows:

$$bl(x,y) = \frac{1}{32}\sum_{a=1}^{5}\sum_{b=1}^{5} p(x-3+a, y-3+b)L(a,b), \tag{1}$$

$$grad_k(x,y) = \frac{1}{16}\sum_{a=1}^{5}\sum_{b=1}^{5} p(x-3+a, y-3+b)G_k(a,b), \tag{2}$$

$$wg(x,y) = max(|grad_k(x,y)|), \quad k = 1,2,3,4, \tag{3}$$

for $1 \leqslant x < R$ and $1 \leqslant y < C$ where R and C are respectively height and width of the image. A weighted low pass mask $L(a,b),\ a,b = 1,\ldots,5$, as given in Fig. 2 is used to evaluate average background luminance in 5×5 window. The maximum weighted gradient of background luminance $wg(x,y)$ around the pixel in four directions is found in the same 5×5 window using mask $G_k(a,b)$ as shown in Fig. 3 for $k = 1,\ldots,4$ and $a,b = 1,\ldots,5$.

Visual model developed from $bl(x,y)$ and $wg(x,y)$ for the calculation of JND profile is summarized by the following equations:

1	1	1	1	1
1	2	2	2	1
1	2	0	2	1
1	2	2	2	1
1	1	1	1	1

Fig. 2. Mask L for calculating average background luminance.

0	0	0	0	0
1	3	8	3	1
0	0	0	0	0
-1	-3	-8	-3	-1
0	0	0	0	0

(a) Mask G_1

0	0	1	0	0
0	8	3	0	0
1	3	0	-3	-1
0	0	-3	-8	0
0	0	-1	0	0

(b) Mask G_2

0	0	1	0	0
0	0	3	8	0
-1	-3	0	3	1
0	-8	-3	0	0
0	0	-1	0	0

(c) Mask G_3

0	1	0	-1	0
0	3	0	-3	0
0	8	0	-8	0
0	3	0	-3	0
0	1	0	-1	0

(d) Mask G_4

Fig. 3. Mask for calculating the weighted gradient $wg(x,y)$ in four directions.

$$s_m(bl(x,y), wg(x,y)) = wg(x,y)\alpha(bl(x,y)) + \beta(bl(x,y)), \tag{4}$$

$$\alpha(bl(x,y)) = 0.0001bl(x,y) + 0.115, \tag{5}$$

$$\beta(bl(x,y)) = \lambda - 0.01bl(x,y), \tag{6}$$

$$v_{th}(bl(x,y)) = \begin{cases} T_0(1-(bl(x,y)/127)^{0.5})) + 3, & \text{for } bl(x,y) \leq 127 \\ \gamma(bl(x,y) - 127) + 3, & \text{for } bl(x,y) > 127 \end{cases} \tag{7}$$

$$JND_1(x,y) = max(s_m(bl(x,y), wg(x,y)), v_{th}(bl(x,y))), \tag{8}$$

where $\alpha(bl(x,y))$ and $\beta(bl(x,y))$ are background luminance dependent functions. s_m in Eq. (4) calculates the spatial masking effect. v_{th} in Eq. (7) calculates the visibility threshold due to the background luminance. Maximum value of s_m and v_{th} gives the distortion threshold value $JND_1(x,y)$ in JND model-1 for the pixel at (x,y) position. The constants T_0, γ and λ are taken as $17, \frac{3}{128}$ and 0.5 respectively for a viewing distance of 6 times the image height [18].

2.1.2. JND Model-2

Previous perceptual model considers only luminance part in an image to determine JND profile. In this perceptual model, along with effects of luminance adaptation, edge accommodative texture masking in spatial domain is also added to meet the HVS characteristic better [19]. An increase in the texture heterogeneity in the background will accommodate more reduction in the visibility of distortion and is referred as texture masking. Accordingly, textured area can mask more deformity than smooth regions. Also error inserted in edge regions is more prominent compared to non-edge areas due to the reality that edge texture drags more attention from a classic HVS. So this modified model explores both edge and non-edge regions along with luminance masking and texture masking.

Perceptual model reflecting the above stated factors is expressed as:

$$JND_2(x,y) = v_{th}(bl(x,y)) + t_m(x,y) - C_g \times min(v_{th}(bl(x,y)), t_m(x,y)), \tag{9}$$

where $JND_2(x,y)$ is the distortion threshold value in JND model-2 at pixel (x,y), $v_{th}(bl(x,y))$ is visibility threshold due to background luminance as defined earlier, $t_m(x,y)$ is texture masking and C_g is the gain reduction component due to overlapping effect in masking

of two basic masking factors for gray level image. Value taken in simulation is 0.3 for viewing distance of approximately 6 times of the image height [19].

Texture masking which considers edge information also is defined as:

$$t_m(x,y) = \varepsilon wg(x,y)W(x,y), \tag{10}$$

where $wg(x,y)$ denotes maximum weighted average of background luminance gradient around the pixel at (x,y) as defined earlier. ε is a control parameter and is set as 0.117. $W(x,y)$ is edge related weight of the pixel at (x,y) and it is computed by Canny edge detector followed by a Gaussian low-pass filter given by:

$$W(x,y) = E(x,y) * g, \tag{11}$$

$E(x,y)$ is edge map of image $p(x,y)$ and is obtained with Canny detector with threshold of 0.5. g is a 7×7 kernel size Gaussian low pass filter with standard deviation of 0.8 to remove noise [20].

2.2. Quantizer

Proposed quantizer depends on the JND profile of the image. In Fig. 1, $f(x,y)$ is the pixel value of input image at (x,y) position and $f_q(x,y)$is the corresponding reconstructed pixel value. $f_q(x,y)$ is given by:

$$f_q(x,y) = q_o \times JND(x,y) \times r(x,y), \tag{12}$$

and

$$r(x,y) = round\left(\frac{f(x,y)}{q_o \times JND(x,y)}\right), \tag{13}$$

q_o is quantization weighting factor and $JND(x,y)$ is either $JND_1(x,y)$ or $JND_2(x,y)$ value. Selection of q_o to have good compression efficiency and visual quality is discussed in Section 3.5.

2.3. Symmetry detection

Human body exhibits bilateral symmetry which is preserved in most of the medical image slices. Function of the proposed symmetry detector is to determine the prominent axis of bilateral symmetry if it exists in the medical image slices. It is achieved by finding collection of mirror feature points [21] in 2-D medical image slices. Using scale invariant feature transform [22], an array of feature points fp_i are identified where $fp_i = (x_i, y_i, \theta_i)$ describes its location in (x,y) co-ordinates and its orientation as θ_i.

First a feature descriptor d_i associated with each feature point is created followed by generation of a set of mirrored descriptors m_i corresponding to d_i. It is realized through reflecting the each image about the x (or y) axis and determining the feature point descriptors m_i for the mirrored image. Every mirrored feature point is a matching feature point of fp_i and hence m_i is the reflected form of d_i. Descriptors d_i and m_i contain the best matching points p_j and p_k that are clustered together to choose a possible symmetry axis. This axis passes perpendicularly through the midpoint of the line joining p_j and p_k. If there are many such potential axis of symmetry, one dominant axis of symmetry is selected on the basis of symmetry magnitude for each pair as predominant axis of symmetry. The major axis of symmetry present in one slice of a medical image is illustrated in Fig. 4.

2.4. Block matching algorithm

As shown in Fig. 1, there are two separate block matching stages in our proposed method. Conventional block matching routine is a way of locating the best match for the macro-blocks in its adjacent image slice. Conventional block matching routine is modified to improve the compression ratio.

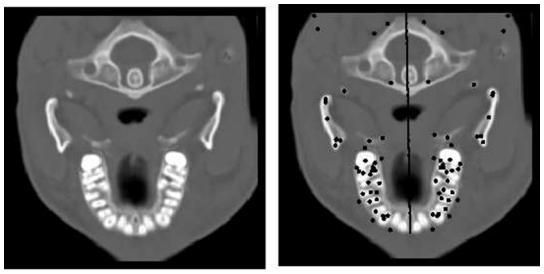

Fig. 4. Symmetry detection: (a) Original image. (b) Image with predominant axis of symmetry.

2.4.1. Inter-slice block matching

Medical image slices generated by imaging modalities are generally cross sections of human body with slices that are parallel to one another separated by a small inter-slice distance. Inter-slice distance would typically be in the range of 5–0.5 mm which results in correlation between the adjacent slices. Inter slice block matching routine is used to improve bit rate by removing these redundancies in slice direction. Current image slice I_i is split into non overlapped blocks of 8×8 and a search window of size 16×16 is defined in the previous image slice I_{i-1}. Most of the medical images have clinically irrelevant background with pixel values of zero. This particular case is considered to improve the efficiency of the compression algorithm by checking for values in 8×8 block. If all values are zero, block match routine is not applied. If all pixel values are not zero in 8×8 block, block match routine is applied to search for a best match in search window. Since there is correlation between the two successive image slices there must be a best match for each 8×8 block in the search window. Sum of Absolute Difference (SAD) given by Eq. (14) for each match is computed.

$$SAD(x,y,r,s) = \sum_{l=0}^{7}\sum_{m=0}^{7}|I_i(x+l,y+m) - I_{i-1}(x+r+l,y+s+m)| \tag{14}$$

where (x,y) is the position of the current block and (r,s) is the displacement of the current block in I_i relative to the block in the previous slice I_{i-1}.

Minimum value of SAD decides the best match. Corresponding block matching residual and displacement vector is taken for further processing. In case, minimum SAD value is greater than sum of all pixel values in the current 8×8 block, pixel values in the 8×8 block are saved instead of saving difference of pixel values in reference window and search window. This particular case is represented by a different displacement vector to assist decoder while reconstructing the image.

2.4.2. Intra-slice block matching

If there is symmetry in the current image plane which is predicted by symmetry detector, inter-slice block matching residual image is split along axis of symmetry. Intra-slice block matching routine is applied on inter-slice block matching residual image. This step is bypassed in case there is no symmetry. Intra-slice block matching is same as inter-slice block matching.

2.5. Entropy coding

Entropy coding is the final lossless step involved to remove the statistical redundancies present in the data. In this method,

entropy coding is achieved by context adaptive binary arithmetic coding (CABAC). CABAC is applied on block matching residual image from inter-slice block matching unit or from intra-slice block matching unit and corresponding displacement vectors. Arithmetic coding tries to evaluate the probability with which certain characters appear and optimize the length of the code. Another advantage of arithmetic coding over other entropy coders is the convenience of adaptation, i.e., update of probability tables as the data is processed.

3. Results and discussions

3.1. Medical data set

The proposed algorithm is tested on a number of image volume data sets obtained from various sources. However, we have presented the results for a total of 704 slices of dataset obtained from Mallinckrodt Institute of Radiology, Image processing lab [23]. The MRI and CT data sets have dimensions of 256×256 with 8 bit per pixel. Table 1 gives the details of the MRI and CT test image data base.

3.2. Metrics for evaluating compression algorithms

Most of the lossy compression algorithms are evaluated by objective metrics such as Peak Signal to Noise Ratio (PSNR) and Relative Error, even though many a time they do not correlate well with subjective quality sensed by the HVS. Visual Signal to Noise Ratio (VSNR), VIF and Structural Similarity Index (SSIM) are some of the HVS based quantitative performance metrics available in the literature [24–26] to evaluate the quality of the reconstructed medical images. The proposed PLIC use VSNR, VIF, SSIM along with PSNR to evaluate the quality of the reconstructed image.

- *VSNR* [27] operates via two stage approach. In the first stage, contrast detection threshold is computed with wavelet based models of visual masking and visual summation to determine the visibility of distortion in the distorted image. If the distortions are below the threshold of detection, VSNR = ∞ (i.e. distorted image is deemed to be of perfect visual fidelity). If the distortions are above the threshold, VSNR value is calculated.
- *SSIM* [28] is based on the assumption that HVS is sensitive to structural information and there is structural dependency among neighboring pixels in the image. This metric estimates the similarity/difference between two images by combining three components of HVS such as brightness, contrast and structure. SSIM index between two images p and g is given by the following expressions [28]:

$$SSIM(p,g) = I(p,g)c(p,g)s(p,g) \tag{15}$$

  where $I(p,g)$ is luminance component, $c(p,g)$ is the contrast component and $s(p,g)$ is the structural component. If images p and g are identical, value of $SSIM(p,g) = 1$ and are close to each other $SSIM(p,g)$ value also close to 1.
- *VIF* [29] quality measure is based on correlation distortion, contrast distortion and luminance distortion. In this quality assessment, the amount of information that can be extracted by brain from the original image is first measured. Later, loss of the same information in the presence of reconstructed (distorted) image is measured. VIF value calculated between original image and its copy is exactly one. For contrast enhanced images, VIF value is more than one. For blurred or compressed images VIF, value lies between 1 and 0.

3.3. Implementation details

The proposed method is implemented in Matlab® 2015a 8.5.0 on an Intel® Core™ i7 Processor. Simulation results for the two JND models discussed are evaluated. Algorithm using JND model-1 is referred as perceptually lossless image coder-1 (PLIC-1) and the algorithm using JND model-2 is referred perceptually lossless image coder-2 (PLIC-2) for further discussions.

3.4. Effect of using JND models in PLIC-1 and PLIC-2

Compression performance of the proposed method in the absence and presence of JND model is given in Table 2. Column 2 and 4 in Table 2 gives the average bit rate after applying only inter-slice block match algorithm without and with modifications in conventional method. There is an improvement of 10.92% in average bit rate by only with inter-slice block matching algorithm. Column 3 and 5 in Table 2 give the average bit rate after applying

Table 1
Details of medical images used in the study [23].

Serial number	Image	History	Number of slices	Image data size
1.	CT Skull	Tripod fracture	192	$256 \times 256 \times 8$
2.	CT wrist	Healing scaphoid dissection	176	$256 \times 256 \times 8$
3.	CT carotid	Internal carotid dissection	64	$256 \times 256 \times 8$
4.	CT Aperts	Aperts syndrome	96	$256 \times 256 \times 8$
5.	MRI Liver t1	Normal	48	$256 \times 256 \times 8$
6.	MRI Liver t2	Normal	48	$256 \times 256 \times 8$
7.	MRI sag head	Left exophthalmos	16	$256 \times 256 \times 8$
8.	MRI ped chest	Congenital heart disease	64	$256 \times 256 \times 8$

Table 2
Comparison of bitrates of methods without and with JND models.

Image	Without modification in block match		With modification in block match		PLIC-1	PLIC-2
	Inter-slice block match	Inter-slice & Intra-slice block match	Inter-slice block match	Inter-slice & Intra-slice block match		
1	2.020	1.983	1.783	1.766	1.767	1.652
2	1.370	1.360	1.163	1.152	1.150	1.137
3	2.158	2.112	1.683	1.654	1.544	1.508
4	1.228	1.207	1.035	0.989	0.783	0.777
5	2.402	2.391	2.383	2.353	2.286	2.282
6	1.946	1.916	1.795	1.794	1.841	1.791
7	1.894	1.884	1.868	1.775	1.572	1.558
8	1.628	1.618	1.645	1.592	1.336	1.336

Table 3
Bit rate and VIF for minimum and maximum value of q_o.

Image set	PLIC-1				PLIC-2			
	bpp_{max}	bpp_{min}	VIF_{max}	VIF_{min}	bpp_{max}	bpp_{min}	VIF_{max}	VIF_{min}
1	1.8131	1.7311	0.9750	0.8498	1.7652	1.6121	0.9811	0.8824
2	1.2294	1.1339	0.9598	0.8192	1.1586	1.1112	0.9600	0.7986
3	1.7382	1.3294	0.9881	0.8776	1.7362	1.2973	0.9900	0.8903
4	0.8810	0.8056	0.9757	0.8719	0.8777	0.7984	0.9770	0.8771
5	2.3992	2.2752	0.9537	0.7789	2.4006	2.2658	0.9539	0.7825
6	1.9894	1.7907	0.9800	0.8679	1.9483	1.7625	0.9866	0.8852
7	1.6166	1.5339	0.9281	0.7331	1.6223	1.5414	0.9287	0.7137
8	1.5076	1.1476	0.9540	0.6350	1.5110	1.1431	0.9540	0.6365

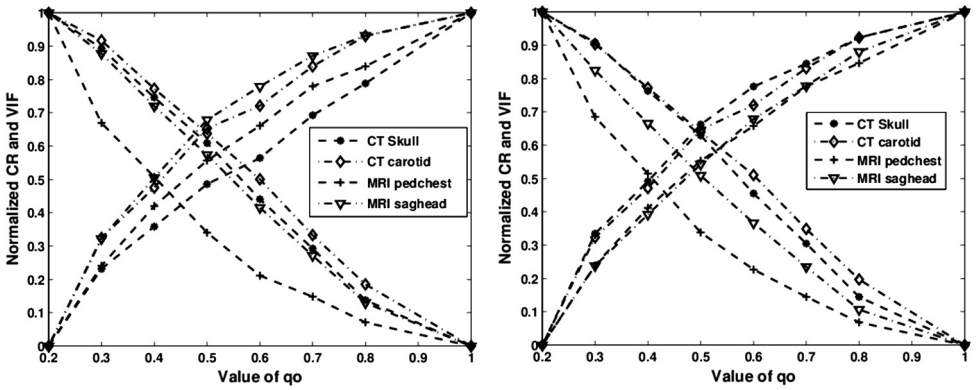

Fig. 5. Variation of VIF and CR with q_o: for (a) PLIC-1 compression technique. (b) PLIC-2 compression technique.

Table 4
Rate-distortion performance of PLIC-1 and PLIC-2.

Image set	PLIC-1					PLIC-2				
	PSNR (dB)	VSNR (dB)	VIF	SSIM	bpp	PSNR (dB)	VSNR (dB)	VIF	SSIM	bpp
1	50.15	46.29	0.9426	1	1.767	51.42	47.94	0.9565	1	1.652
2	48.98	53.53	0.9145	1	1.150	49.05	53.56	0.9169	1	1.137
3	52.89	50.88	0.9700	1	1.544	53.46	50.89	0.9710	1	1.508
4	52.14	56.37	0.9481	0.9994	0.783	52.28	56.42	0.9503	0.9994	0.777
5	42.64	46.69	0.8927	0.9947	2.286	42.67	46.69	0.8937	0.9947	2.282
6	50.53	46.98	0.9508	1	1.841	51.20	47.04	0.9597	1	1.791
7	46.39	55.32	0.8543	1	1.572	46.42	55.35	0.8550	1	1.575
8	43.30	54.29	0.8334	0.9914	1.336	43.32	54.28	0.8337	0.9914	1.336

inter-slice block match and intra-slice block match algorithm if symmetry is present in slice, without and with modifications in conventional method. There is an average improvement of 12.18% in average bit rate in overall performance of lossless compression algorithm with modifications in block match routine.

3.5. HVS based performance evaluation

Algorithm is evaluated for different values of quantization weighting factor q_o ranging from 0.2 to 1 in steps of 0.1. This demonstrates that as the value of q_o increases, quality of reconstructed image decreases and compression gain increases. Corresponding maximum and minimum value of bit rate and VIF are tabulated in Table 3. By measuring the quality of reconstructed image, value of q_o can be adjusted.

Normalized Compression Ratio (CR) and VIF are plotted for range of q_o values from 0.2 to 1 as shown in Fig. 5. As value of q_o increases, CR increases and VIF decreases. Nearest value of q_o where CR and VIF curves meet is considered the best value to get both good bit rate and visual quality. Value of q_o is found to be 0.5 for all data sets except for MRI ped chest. Value of $q_o = 0.4$ is used for MRI ped chest to have good bit rate and visual quality as seen from the graph.

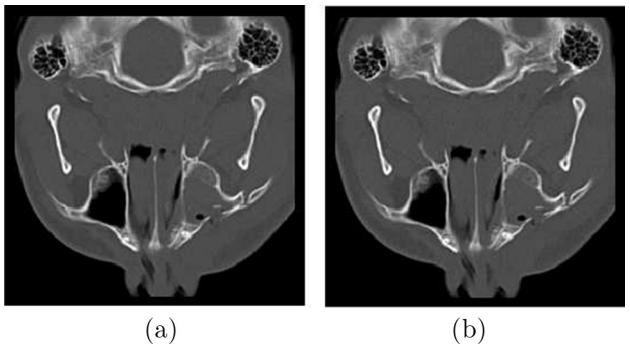

Fig. 6. Visual clip of original and reconstructed CT Skull images with PLIC-2 compression technique (slice number of image is 40) at bpp = 1.652; PSNR = 51.42 dB; SSIM = 1; VIF = 0.9565.

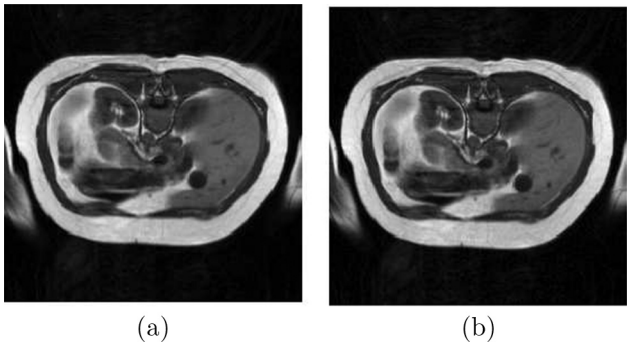

Fig. 7. Visual clip of original and reconstructed MRI Liver t1 images with PLIC-2 compression technique (slice number of image is 20) at bpp = 2.282; PSNR = 42.67 dB; SSIM = 0.9947; VIF = 0.8937.

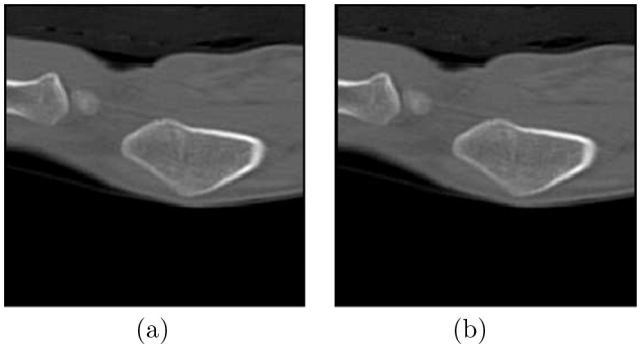

Fig. 8. Visual clip of original and reconstructed CT Wrist images with PLIC-2 compression technique (slice number of image is 20) at bpp = 1.137; PSNR = 49.05 dB; SSIM = 1; VIF = 0.9169.

By varying the value of q_0 in Eq. (12), various bit rates can be obtained for various quality of reconstructed image. Quality is measured with PSNR as well as HVS based metrics like VSNR, VIF and SSIM metrics. The rate-distortion performance comparison for PLIC-1 and PLIC-2 are shown in Table 4. SSIM yields the best performance indicator of image quality and it gives the closest match to the subjective quality [30]. A sample of original medical image slice from each data sets and corresponding reconstructed image with PLIC-2 compression technique is shown in Figs. 6–8.

Subjective evaluation was performed in order to confirm the visual quality of the reconstructed data. Six observers were from the medical field which included radiologists and radiographers. A questionnaire was prepared for all the dataset listed in the Table 1. Test condition set for the image data was at quantization weighting factor q_o of 0.5. The objective quality and the subjective score at the specified bit rate for each of the data used for subjective evaluation is listed in Table 5. The observers were shown the original and reconstructed image and were asked to rate the quality on a scale of 1–5. A score of 1 represents poor and 5 represents excellent. The medical experts were satisfied with the quality of reconstructed image and have confirmed that there is no visual impairment that would hinder the medical diagnosis.

3.6. Performance comparison with lossless coders

Although, the proposed method is a perceptually lossless method, we compare its compression performance with that of 3-D lossless compression techniques- namely Context based Adaptive Lossless Image Coder (CALIC) [31], 3-D JPEG [32], 3-D EZW [23], 3-D CB EZW [23], Medical Images Lossless Compression (MILC) [7], HEVC Intra mode [13], HEVC random access mode [13] and PLC [33]. Table 6 compares the bitrates of PLIC-1 and PLIC-2 with other lossless compression methods.

CALIC is an adaptive predictive model used for the lossless compression of static 2-D images even though it is computationally complex. In this technique, there is no effort to remove redundancy in slice direction. 3-D EZW use 3-D wavelet transform to remove statistical dependency in all three directions. 3-D CB-EZW algorithm employs context modeling. PLC is a symmetry and differential pulse-code modulation based perceptually lossless image coder for volumetric compression of MR and CT medical images. Fig. 9 shows the percentage increase in bit rate with reference method against the algorithm yielding the best bit-rate for each of the test data sets. The results show that the removal of perceptual redundancy and dependency in the slice direction significantly

Table 5
Objective and subjective evaluation of PLIC-2; score allotted: excellent-5; very good-4; good-3; average-2; poor-1.

Image	bpp	Objective measure			Score	
		PSNR (dB)	VIF	SSIM	Radiologists score	Radiographers score
CT Skull; Slice-1	1.651	51.41	0.956	1	5	5
CT Skull; Slice-20	1.651	51.41	0.956	1	5	5
CT Skull; Slice 50	1.652	51.42	0.956	1	5	5
CT wrist; Slice 15	1.137	49.05	0.916	1	5	5
CT wrist; Slice 30	1.136	49.05	0.916	1	5	5
CT wrist; Slice 50	1.137	53.56	0.916	1	5	5
CT carotid; Slice 10	1.510	50.88	0.971	1	5	5
CT carotid; Slice 30	1.509	50.89	0.971	1	5	5
CT carotid; Slice 50	1.511	50.89	0.971	1	5	5
CT Aperts; Slice 20	0.775	56.41	0.951	0.999	5	5
CT Aperts; Slice 40	0.776	56.41	0.951	0.999	5	5
CT Aperts; Slice 60	0.775	56.40	0.951	0.999	5	5
MRI Liver t1; Slice 05	2.280	42.66	0.893	0.993	5	5
MRI Liver t1; Slice 25	2.281	42.67	0.893	0.994	5	5
MRI Liver t2; Slice 05	1.791	51.20	0.959	1	5	5
MRI Liver t2; Slice 40	1.790	51.20	0.959	1	5	5
MRI sag head; Slice 5	1.572	46.40	0.855	1	5	5
MRI sag head; Slice 10	1.574	46.41	0.855	1	5	5
MRI ped chest; Slice 25	1.335	43.31	0.833	0.9912	5	5
MRI ped chest; Slice 40	1.336	43.32	0.833	0.9914	5	5

Table 6
Comparison of bit rates (bpp) of PLCs with other methods.

Image	CALIC[31]	3-DEZW [23]	3-DCB EZW [23]	3-D JPEG [32]	MILC [7]	HEVC Intra [13]	HEVC RA [13]	PLC [33]	PLIC-1	PLIC-2
1	2.725	2.357	2.200	3.112	2.030	3.083	1.905	2.028	1.767	1.652
2	1.691	1.394	1.272	1.652	1.066	2.195	1.155	1.131	1.150	1.137
3	1.654	1.601	1.527	1.965	1.358	2.198	1.586	1.406	1.544	1.508
4	1.047	1.060	0.987	1.238	0.819	1.289	0.825	0.903	0.783	0.777
5	3.047	2.545	2.398	3.125	2.196	3.742	2.391	1.921	2.286	2.282
6	2.243	1.944	1.822	2.622	1.759	2.811	1.725	1.766	1.841	1.791
7	2.585	2.322	2.227	2.758	2.097	2.732	1.873	1.669	1.572	1.558
8	2.810	2.176	2.022	2.768	1.655	3.352	1.700	1.742	1.336	1.336

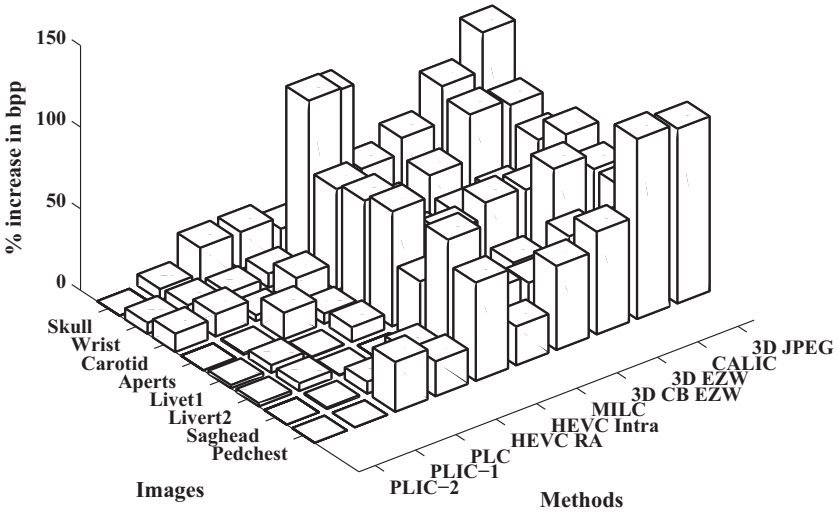

Fig. 9. Percentage increase in bit rate with reference method against the algorithm yielding the best bit-rate for each test data set.

improves performance. The proposed methods show better performance when compared to CALIC, EZW, CB EZW, 3-D JPEG and MILC for most of the test data sets. The bit rate is improved by 46.44% and 49.06% on average in case of PLIC-1 and PLIC-2 respectively compared to 2-D based CALIC. If one takes the PLIC-2 as the reference for average increase in percentage bit rate, PLIC-1 yields almost similar result, since the difference between the two is 2.25%. MILC coder provide result with an average difference in bit rate of 8.12%. The average difference increases up to 19.83% and 63.47% for 3-D CB EZW and 3-D JPEG coder. Comparison of PLIC-2 coder with HEVC Intra and HEVC-RA coder provide an average difference in bit rate of 79.81% and 10.29% respectively.

3.7. Performance comparison with lossy coders

The performance of the algorithms is also compared with lossy state-of-the-art coders like JPEG2000 Part 1 and JPEG2000 Part 2. The rate-distortion value for each of the dataset and the methods are given in Tables 7–9. Kakadu 7.4 version software is used for the implementation of JPEG-2KP1 and JPEG-2KP2 [34]. From the values in the table, it is clearly seen that PLIC-1 and PLIC-2 give a better quality either at nearly same or lower bitrates. Tables 8 and 9 show that the quality of the reconstructed image of our coder has better quality in terms of HVS metrics without any perceivable visual distortion.

Table 7
Comparison of PSNR of JPEG-2K Part 1, JPEG-2K Part 2, PLIC-1 and PLIC-2 for various bitrates.

Image set	J2K-P1		J2K-P2		PLIC-1		PLIC-2	
	bpp	PSNR (dB)	bpp	PSNR (dB)	bpp	PSNR (dB)	bpp	PSNR (dB)
1	1.664	49.17	1.684	49.17	1.654	50.87	1.648	50.59
2	1.261	53.78	1.281	52.89	1.229	52.93	1.224	53.01
3	1.702	55.99	1.707	55.97	1.7384	58.23	1.736	59.24
4	0.914	56.85	0.901	56.97	0.881	56.50	0.877	56.62
5	1.957	49.20	1.977	49.30	2.399	47.23	2.400	47.28
6	2.240	55.96	2.260	55.84	1.790	55.12	1.762	55.89
7	1.590	48.23	1.592	48.86	1.616	50.13	1.622	50.15
8	1.559	48.46	1.579	48.52	1.507	48.66	1.511	48.68

Table 8
Comparison of SSIM of JPEG-2K Part 1, JPEG-2K Part 2, PLIC-1 and PLIC-2 for various bitrates.

Image set	J2K-P1		J2K-P2		PLIC-1		PLIC-2	
	bpp	SSIM	bpp	SSIM	bpp	SSIM	bpp	SSIM
1	1.664	0.99001	1.684	0.99002	1.654	1	1.648	1
2	1.261	0.9977	1.281	0.9976	1.229	1	1.224	1
3	1.702	0.9976	1.707	0.9986	1.7384	1	1.736	1
4	0.914	0.9963	0.901	0.9970	0.881	1	0.877	1
5	1.957	0.9926	1.977	0.9937	2.399	1	2.400	1
6	2.240	0.9988	2.260	0.9979	1.790	1	1.762	1
7	1.590	0.9967	1.592	0.9983	1.616	1	1.622	1
8	1.559	0.9918	1.579	0.9918	1.507	1	1.511	1

Table 9
Comparison of VIF of JPEG-2K Part 1, JPEG-2K Part 2, PLIC-1 and PLIC-2 for various bitrates.

Image set	J2K-P1		J2K-P2		PLIC-1		PLIC-2	
	bpp	VIF	bpp	VIF	bpp	VIF	bpp	VIF
1	1.664	0.9151	1.684	0.9151	1.654	0.9405	1.648	0.9489
2	1.261	0.9704	1.281	0.99703	1.229	0.9767	1.224	0.9825
3	1.702	0.9780	1.707	0.9784	1.7384	0.9881	1.736	0.99
4	0.914	0.9784	0.901	0.9792	0.881	0.9757	0.877	0.9770
5	1.957	0.9528	1.977	0.9535	2.399	0.9537	2.400	0.9539
6	2.240	0.9863	2.260	0.9841	1.790	0.98	1.762	0.9866
7	1.590	0.9199	1.592	0.9207	1.616	0.9281	1.622	0.9287
8	1.559	0.9170	1.579	0.9170	1.507	0.954	1.511	0.9540

4. Conclusion

In this paper, we have proposed two 3-D perceptually lossless coders for medical image dataset. Inter-slice block matching applied removes any redundancies between the adjacent slices, thus addressing the volumetric coding of image data. Since most of the medical images have inherent bilateral symmetry, these are removed by a symmetry detector and intra-slice block matching.

In this work, two JND models based on HVS have been proposed to remove perceptual redundancies. Visibility threshold in JND-1 depends on average background luminance around the pixel and spatial gradient in the background luminous gradient, where as JND-2 depends on an additional texture masking. From the results, it has been shown that additional compression is achieved by using texture masking in JND-2. As the work proposes to remove perceptually redundant data, we have used HVS based quality metrics like VIF, SSIM and VSNR to evaluate the quality of the reconstructed image. Optimum value of quantizer threshold q_0 is chosen by evaluating the rate-distortion performance of the two PLICs. The quality measures like PSNR, VSNR, VIF and SSIM for various bitrates computed for PLIC-1 and PLIC-2 show that these achieve good compression for higher values of PSNR and VSNR. SSIM in most of the cases are 1 or very close to 1, indicating that human eye can not distinguish between original and reconstructed image.

The compression performance of PLIC-1 and PLIC-2 is compared with that of lossless coders like CALIC, 3-D-EZW, 3-D CB EZW, MILC, HEVC Intra, HEVC-RA and PLC. From the results obtained, it is observed that our method achieves better compression without introducing any perceivable loss. Also rate-distortion performance comparison of PLIC-1 and PLIC-2 has been made with that of lossy state-of-the-art coders like JPEG2000 Part 1 and JPEG2000 Part 2. PSNR, VSNR,VIF and SSIM for various bitrates for each of the methods were calculated. From these, it has been observed that our method provides lower or same bitrates for a better quality of reconstructed image.

Thus by using JND models, we have achieved perceptually lossless compression without any loss of diagnostically significant data which will be a big milestone in the medical field. Future extension of this work can be to adapt this to a lossless-to-lossy framework by introducing scalability. Scalability is desirable for field like tele-medicine where in the medical experts can download the data at very low bitrates but can get more information when required at higher bitrates. Moreover as there is no difference between original and compressed images, subjective evaluation is rated as excellent by radiologists.

Acknowledgments

The authors would like to thank Prof. A. Bilgin, Department of Electrical and Computer Engineering, University of Arizona, Tucson, USA for providing us the medical image data sets.

References

[1] A. Tzannes, Compression of 3-Dimensional Medical Image Data using Part 2 of JPEG 2000, Aware. Inc, November 2000.
[2] W. Yodchanan, Lossless compression for 3-D MRI data using reversible KLT, in: IEEE International Conference on Audio, Language and Image Processing, 2008, pp. 1560–1564.
[3] G. Menegaz, J. Thiran, Three-dimensional encoding/two-dimensional decoding of medical data, IEEE Trans. Med. Imag. 22 (2003) 424–440.
[4] V. Sanchez, R. Abugharbieh, P. Nasiopoulos, Symmetry-based scalable lossless compression of 3D medical image data, IEEE Trans. Med. Imag. 28 (2009) 1062–1072.
[5] V. Sanchez, R. Abugharbieh, P. Nasiopoulos, 3D scalable lossless compression of medical images based on global and local symmetries, in: 16th IEEE International Conference on Image Processing, 2009, pp. 2525–2528.
[6] S. Amraee, N. Karimi, S. Samavi, S. Shirani, Compression of 3D MRI images based on symmetry in prediction-error field, in: IEEE International Conference on Multimedia and Expo., 2011, pp. 1–6.
[7] R. Pizzolante, B. Carpentieri, Lossless, low-complexity, compression of three-dimensional volumetric medical images via linear prediction, in: 18th IEEE International Conference on Digital Signal Processing, 2013, pp. 1–6.
[8] D.A. Clunie, Lossless compression of grayscale medical images: effectiveness of traditional and state of the art approaches, in: Medical Imaging 2000, International Society for Optics and Photonics, 2000, pp. 74–84.
[9] S.-G. Miaou, F.-S. Ke, S.-C. Chen, A lossless compression method for medical image sequences using JPEG-LS and interframe coding, IEEE Trans. Inform. Technol. Biomed. 13 (5) (2009) 818–821.
[10] C. Yan, Y. Zhang, J. Xu, F. Dai, L. Li, Q. Dai, F. Wu, A highly parallel framework for HEVC coding unit partitioning tree decision on many-core processors, IEEE Sign. Process. Lett. (2014) 573–576.

[11] C. Yan, Y. Zhang, J. Xu, F. Dai, J. Zhang, Q. Dai, F. Wu, Efficient parallel framework for HEVC motion estimation on many-core processors, IEEE Trans. Circ. Syst. Video Technol. 24 (2014).
[12] V. Sanchez, Joan Bartrina-Rapesta, Lossless compression of medical images based on HEVC intra coding, in: IEEE International Conference on Acoustics, Speech and Signal Processing, 2014, pp. 6622–6626.
[13] J.M. Santos, A.F.R. Guarda, Nuno M.M. Rodrigues, S.M.M. Faria, Contributions to lossless coding of medical images using minimum rate predictors, IEEE International Conference on Image Processing, 2014.
[14] D. Wu, D. Tan, M. Baird, J. DeCampo, C. White, H. Wu, Perceptually lossless medical image coding, IEEE Trans. Med. Imag. 25 (2006) 335–344.
[15] M.J. Nadenau, S. Winkler, D. Alleysson, M. Kunt, Human vision models for perceptually optimized image processing – a review, Proc. IEEE (2000) 1–32.
[16] A.K. Jain, Fundamentals of Digital Image Processing, Prentice-Hall, Inc., 1989.
[17] R.J. Safranek, J.D. Johnston, A perceptually tuned sub-band image coder with image dependent quantization and post-quantization data compression, in: International Conference on Acoustics, Speech, and Signal Processing, IEEE, 1989.
[18] C.H. Chou, Y.C. Li, A perceptually tuned subband image coder based on the measure of just-noticeable-distortion profile, IEEE Trans. Circ. Syst. Video Technol. 5 (1995) 467–476.
[19] X. Yang, W. Ling, Z. Lu, E.P. Ong, S. Yao, Just noticeable distortion model and its applications in video coding, Sign. Process.: Image Commun. 20 (2005) 662–680.
[20] J. Canny, A computational approach to edge detection, IEEE Trans. Pattern Anal. Mach. Intell. 6 (1986) 679–698.
[21] G. Loy, J.-O. Eklundh, Detecting symmetry and symmetric constellations of features, in: Computer Vision Conference, 2006, pp. 508–521.
[22] D.G. Lowe, Distinctive image features from scale-invariant keypoints, Int. J. Comput. Vis. 60 (2004) 91–110.
[23] A. Bilgin, G. Zweig, M.W. Marcellin, Efficient lossless coding of medical image volumes using reversible integer wavelet transforms, in: IEEE Conference Proc. on Data Compression, 1998.
[24] M. Razaak, M.G. Martini, K. Savino, A study on quality assessment for medical ultrasound video compressed via HEVC, IEEE J. Biomed. Health Infor. 18 (2014) 1552–1559.
[25] I.A. Kowalik-Urbaniak, J. Castelli, N. Hemmati, D. Koff, N. Smolarski-Koff, E.R. Vrscay, J. Wang, Z. Wang, Modelling of subjective radiological assessments with objective image quality measures of brain and body CT images, in: Image Analysis and Recognition, 2015, pp. 3–13.
[26] Z. Al-Ameen, G. Sulong, Deblurring computed tomography medical images using a novel amended landweber algorithm, Interdiscipl. Sci.: Comput. Life Sci. 7 (2015) 319–325.
[27] D.M. Chandler, S.S. Hemami, VSNR: a wavelet-based visual signal-to-noise ratio for natural images, IEEE Trans. Image Process. 16 (2007) 2284–2298.
[28] Z. Wang, A.C. Bovik, H.R. Sheikh, E.P. Simoncelli, Image quality assessment: from error visibility to structural similarity, IEEE Trans. Image Process. 13 (2004) 600–612.
[29] H.R. Sheikh, A.C. Bovik, Image information and visual quality, IEEE Trans. Image Process. 15 (2006) 430–444.
[30] I. Kowalik-Urbaniak, D. Brunet, J. Wang, D. Koff, N. Smolarski-Koff, E.R. Vrscay, B. Wallace, Z. Wang, The quest for 'diagnostically lossless' medical image compression: a comparative study of objective quality metrics for compressed medical images, in: Medical Imaging, International Society for Optics and Photonics, 2014, pp. 903717–903728.
[31] X. Wu, N. Memon, CALIC – a context based adaptive lossless image codec, in: IEEE International Conference Proc. on Acoustics, Speech, and Signal Processing, vol. 4, 1996, pp. 1890–1893.
[32] S. Ait Aoudia, F.Z. Benhamida, M.A. Yousfi, Lossless compression of volumetric medical data, in: Computer and Information Sciences, 2006, pp. 563–571.
[33] B.K. Chandrika, P. Aparna, D. Sumam, Symmetry based perceptually lossless compression of 3D medical images in spatial domain, in: International Conference on Computer, Communication, and Control Technology, 2014, pp. 53–57.
[34] KAKADU, KAKADU Version 7.4 JPEG2000 Software Development Tool Kit. <http://kakadusoftware.com/>, 2016 (accessed on May 2016).